Journal of the European Ceramic Society **19** (1999) 227–237

PII: S0955-2219(98)00184-8
0955-2219/98/$—see front matter

Asymmetric Tensile and Compressive Creep Deformation of Hot-isostatically-pressed Y_2O_3-Doped -Si_3N_4†

Andrew A. Wereszczak,[a]* Mattison K. Ferber,[a] Timothy P. Kirkland,[a] Amy S. Barnes,[a]‡ Edward L. Frome[a]§ and Mamballykalathil N. Menon[b]

[a]High Temperature Materials Laboratory, Oak Ridge National Laboratory, Oak Ridge, TN 37831-6069, USA
[b]Allied Signal Engines, Allied Signal Aerospace Company, Phoenix, AZ 85072, USA

(Received 20 April 1998; revised version received 17 July 1998; accepted 31 July 1998)

Abstract

The uniaxial tensile and compressive creep rates of an yttria-containing hot-isostatically-pressed silicon nitride were examined at several temperatures between 1316 and 1399°C and found to have different stress dependencies. Minimum creep rates were always faster in tension than compression for an equal magnitude of stress. An empirical model was formulated which represented the minimum creep rate as a function of temperature for both tensile and compressive stresses. The model also depicted the asymmetric creep deformation using exponential and linear dependence on tensile and compressive stress, respectively. Unlike other models which represent either tensile or compressive creep deformation as a respective function of tensile or compressive stress, the model in the present study predicted creep deformation rate for both tensile and compressive stresses without conditional or a priori *knowledge of the sign of stress. A statistical weight function was introduced to improve the correlation of the model's regressed fit to the experimental data. Post-testing TEM microstructural analysis revealed that differences in the amount of tensile- and compressive-stress-induced cavitation accounted for the creep strain asymmetry between them, and that cavitation initiated in tensile and compressively crept specimens for magnitudes of creep strain in excess of 0·1%.*

Keywords: Si_3N_4, creep, electron microscopy, mechanical properties, modelling.

1 Introduction

The need to characterize, understand, and model both tensile and compressive creep of structural ceramics, such as silicon nitride (Si_3N_4), arises from the considerably lower creep rates exhibited by these materials in compression than in tension for equivalent magnitudes in stress.[1,2] Such modeling needs to acknowledge the asymmetrical creep to accurately predict and interpret stress state changes and dimensional redistribution in load-bearing components and standard test coupons at elevated temperatures (e.g., nozzles and blades in advanced gas turbine engines, flexure bars, etc.).

Several models have been used to describe or predict either the tensile or compressive creep deformation of polycrystalline ceramics. Traditionally the power-law Norton–Bailey–Arrhenius (NBA) model [3] is used,

$$\mathrm{d}\varepsilon/\mathrm{d}t = A_{\mathrm{nb}}\sigma^n \exp(-Q/RT) \qquad (1)$$

where A_{nb} is a constant, σ is stress, n is the stress-exponent, Q is activation energy, R is the gas constant, and T is absolute temperature. The NBA model represents compressive creep data of silicon nitride well[1,2,4,5] where n typically equals 1 for

*To whom correspondence should be addressed: Fax: +1-423-574-6098.
†Research supported by three sources: (a) US Department of Energy Contract No. 86X-SC674C, 'Life Prediction Methodology for Ceramic Components of Advanced Heat Engines,' WBS Element 3.2.2.3; Assistant Secretary for Energy Efficiency and Renewable Energy, Office of Transportation Technologies, as part of the (b) High Temperature Materials Laboratory Fellowship Program; and (c) Heavy Vehicle Propulsion System Materials Program, Oak Ridge National Laboratory, managed by Lockheed Martin Energy Research Corporation for the US Department of Energy under contract number DE-AC05-96OR22464.
‡Currently in the graduate program of the Department of Materials Science and Engineering, Pennsylvania State University, University Park, PA, USA.
§Computational Mathematics and Statistics Section, Computer Science and Mathematics Division.

rate-limiting Coble creep.[6] The NBA model has also been extensively used for tensile creep data as well with n typically being greater than unity due to cavitation.[1,2,4,7–11] However, the portrayal of tensile creep data by eqn (1) has been brought into question the last few years for silicon nitride. Recent interpretations of tensile creep rate data have shown that the power-law formulation of eqn (1) does not satisfactorily represent its dependence on stress (stress exponent value is dependent on the value of applied stress), and that an exponential representation is more suitable.[2,4,12] A representation of tensile creep rate exponentially dependent on stress has the form,[13]

$$\mathrm{d}\varepsilon/\mathrm{d}t = A_e \exp(B_e\sigma)\exp(-Q/RT) \qquad (2)$$

where A_e and B_e are constants. A similar exponential-type model which represents tensile creep rate as following a hyperbolic sine dependence on stress has been used.[9,14,15] It can be shown that for relatively low stresses that the hyperbolic sine function simplifies to the power-law form in eqn (1) and that it simplifies to the exponential form of eqn (2) for relatively high stresses. A disadvantage of the hyperbolic sine function representation is it is symmetric and consequentially predicts the magnitudes of compressive and tensile creep rates to be equal for equally applied magnitudes of stress.

More recently, another exponential-type model has been proposed in which the tensile creep rate is represented as a function of stress according to[16–18]

$$\mathrm{d}\varepsilon/\mathrm{d}t = A_N\sigma \exp(B_N\sigma)\exp(-Q/RT) \qquad (3)$$

where A_N and B_N are constants. For this model, the exponential dependence of creep rate on stress results from the kinetics of the secondary phase redistribution from growing cavities. Increasing stress initiates larger concentrations of cavities, which in turn increases the creep rate. The exponential stress term in eqn (3) is found to approximate the stress dependency of the number of cavitation sites.

A limitation of the models represented by eqns (1)–(3) is they cannot be singly used to accurately portray *both* tensile and compressive creep rate data as a function of stress. The NBA model has been used for both tensile and compressive creep rate data; however, the stress-exponents are almost always different for tension and compression, so two different forms of eqn (1) must be used with the n values being differently-valued for each.[19] This becomes inconvenient for modeling multiaxial creep deformation when both tensile and compressive stresses may be present because one must conditionally know *a priori* the sign of stress in order to use the proper stress exponent in eqn (1).[20] Disadvantages of eqn (2) include the lack of linear dependence of compressive creep rate on compressive stress and that a finite creep rate is predicted for zero stress. Although eqn (3) predicts zero creep rate for zero stress, it does not represent compressive creep rate as being linear with compressive stress.

The motivations behind the present study were to (1) formulate a model which would represent both tensile and compressive creep deformation as

Table 1. Summary of minimum creep rate as a function of temperature and stress

Temperature (°C)/(°F)	*Stress* (MPa)/(ksi)	*Minimum creep rate* ($\times 10^{-10}s^{-1}$)
1316/2400	40/5·8	5·6
	75/10·9	8·0
	125/18·1	18
	−125/−18·1	−2·9
	−200/−29·0	−2·4
	−300/−43·5	2·7
	−400/−58·0	−9·3
	−500/−72·5	−10
1343/2450	−300/−43·5	−9·3
	−400/−58·0	−12
	−500/−72·5	−16
1371/2500	30/4·4	5·3
	60/8·7	28
125/18·1	50	
	130/18·9	87
	135/19·6	63
	140/20·3	68
	145/21·0	110
	145/21·0	160
	145/21·0	150
	145/21·0	140
	145/21·0	100
	145/21·0	100
	145/21·0	110
	145/21·0	110
	145/21·0	110
	180/26·1	470
	180/26·1	420
	180/26·1	260
	180/26·1	300
	190/27·6	230
	−30/−4·4	−2·8
	−100/−14·5	−5·3
	−200/−29·0	−12
	−300/−54·5	−11
	−400/−58·0	−18
	−500/−72·5	−13
1399/2550	35/3·6	12
	85/12·3	50
	90/13·1	59
	100/14·5	130
	110/16·0	130
	125/18·1	140
	130/18·9	230
	130/18·9	240
	140/20·3	330
	150/21·8	320
	−25/−3·6	−2·7
	−50/−7.3	−8·4
	−100/−14·5	−10
	−200/−29·0	−16
	−300/−43·5	−21

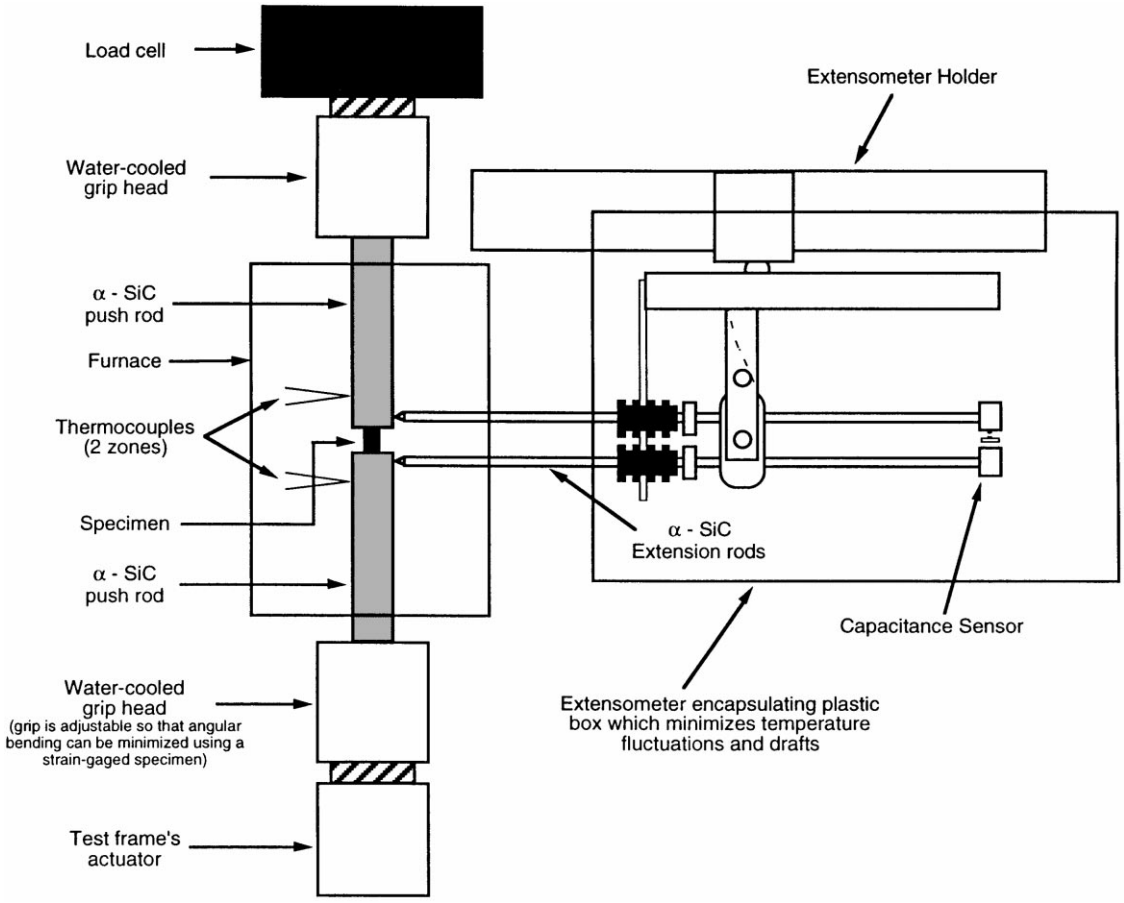

Fig. 1. Schematic of compression creep test. A cylindrical specimen geometry was used having a length and diameter of 10 and 5 mm, respectively.

a function of stress and temperature without conditional or *a priori* knowledge of the sign of stress, (2) generate an appreciably-sized tensile and compressive creep database for a polycrystalline structural ceramic to statistically facilitate the first goal, and (3) perform microstructural examinations on pre- and post-tested specimens to explain the asymmetric creep behavior.

2 Material, Test Procedures, and Analysis

The examined Si_3N_4 was an yttria-doped (4 wt%) hot-isostatically-pressed material designated as NT154.* All tensile and compressive specimens were machined from billets made from the same processing batch. NT154 is comprised of long, acicular-shaped grains ($\approx 5\,\mu$m long, aspect ratio ≈ 10), mixed with equiaxed grains (having a diameter of 0·3 to 0·5 μm). NT154 has approximately 10% α-Si_3N_4 and 90% β-Si_3N_4 in its as-received state; however, at the test conditions examined in the present study, the remnant 10% α-Si_3N_4 converted to β-Si_3N_4.[7,8] NT154 has stable crystalline yttrium silicate secondary phases at elevated temperatures. It has an average room temperature tensile and flexure (ASTM C1161-B[21]) strength of 759 (100 specimens) and 915 MPa (60 specimens), respectively.[22] Several high temperature mechanical testing studies have been reported with this material.[2,4,7,8,10,11]

The test frame for the compression creep tests was comprised of components capable of operating at high temperatures and compressive loads, and which permitted the minimization of axial bending through appropriate load-train adjustments. The compression creep test setup is illustrated in Fig. 1. The load train consisted of two fully-dense α-silicon carbide (SiC) push-rods, 19·05 mm in diameter and 76 mm long, attached to water cooled grips in a servo-hydraulic test machine. A cylindrical test specimen (10 mm long and 5 mm in diameter) was compressed between the free, axially-aligned, flat and parallel ends of the SiC push-rods. The choice of an aspect ratio of two was a compromise of minimal likelihood of buckling and barreling.[23] A strain-gaged specimen was used in concert with load-train-axial-adjusters at room temperature to minimize axial bending strains; the maintenance of minimal bending between tests was interpreted to

*Saint-Gobain/Norton Industrial Ceramics Corporation, Northboro, MA.

signify that axial bending strains remained minimal during high temperature testing. The specimen and the SiC pushrods were heated with a short, resistance-heated furnace (50 mm vertical hot zone) to the setpoint temperature. Two thermocouples positioned close to the specimen were used to monitor and control the setpoint temperature to within $\pm 3°C$. A high-temperature capacitive extensometer (25 mm gage length) was used to measure the mutual displacements of the SiC loading push-rods to a resolution of $\pm 0{\cdot}2\,\mu m$ during static loading creep tests. Inspection of the α-SiC push-rods after every test showed no evidence of their deformation, so compressive creep displacements measured with the extensometer were attributed entirely to the creeping specimen. These displacements were measured as a function of time using a personal computer. Test temperatures were 1316, 1343, 1371, and 1399°C, and examined static compressive stresses ranged between 25 and 500 MPa. Tests were terminated after at least 100 h of secondary creep, so a typical whole test duration was 150–200 h. The compressive creep histories showed a primary and secondary creep region. Tertiary creep was never observed. The minimum compressive creep rate from the secondary creep region was determined as a function of stress and temperature for each specimen.

The higher-stress tensile creep results were excerpted from previous NT154 creep studies;[7,8,22] however, additional tensile creep tests were performed in the present study at mid- and low-valued stresses. A schematic of the tensile creep test set-up is illustrated in Fig. 2. This tensile test apparatus utilized many of the same test hardware components as the compressive creep tests. A buttonhead specimen geometry (gage length and diameter of 35 and 6·35 mm, respectively) was used. The same test facility and specimen geometry were also used to generate the high tensile stress creep data which were excerpted from Refs. 7, 8 and 22. Passive self-aligning grips were used to minimize load train bending. A high temperature contacting extensometer (25 mm gage length) was used to continuously measure creep strain. Tensile displacements were measured as a function of time using a personal

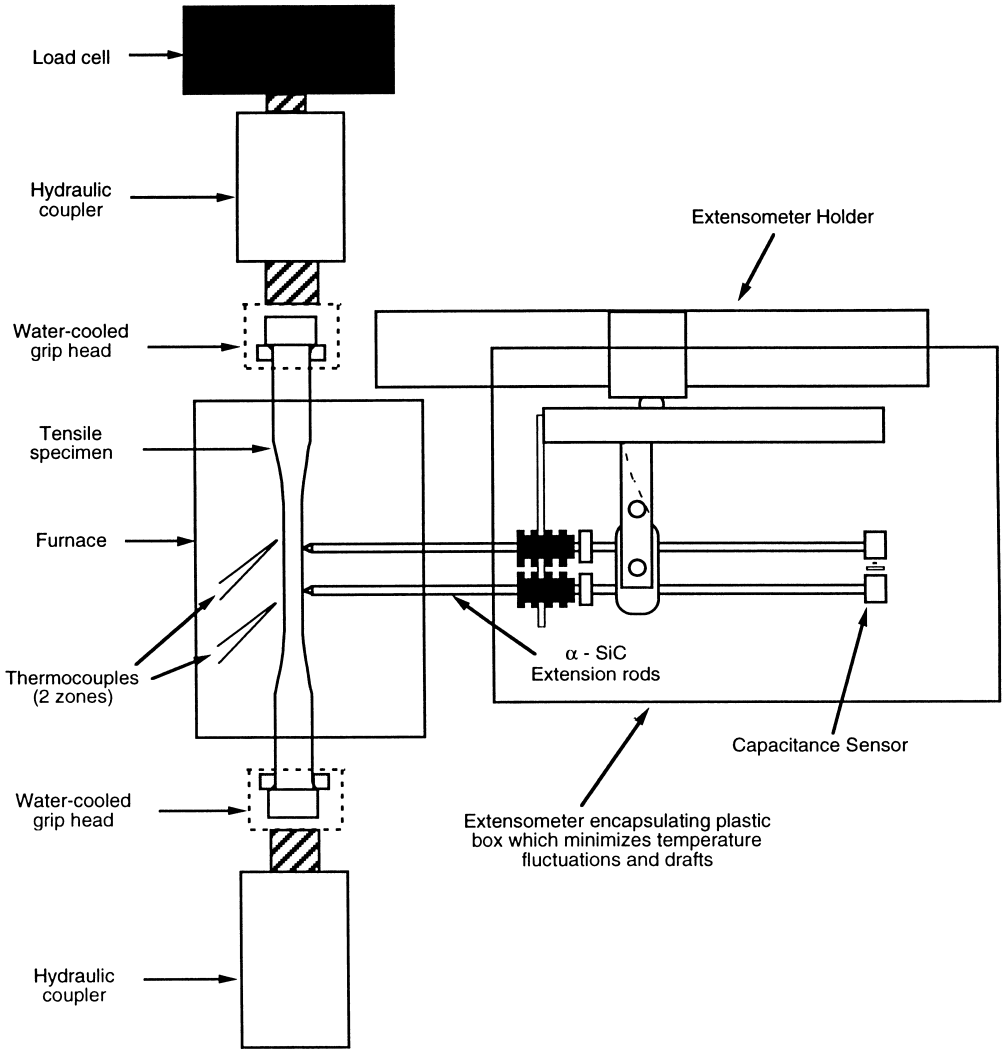

Fig. 2. Schematic of tensile creep test. A buttonhead specimen geometry was used having a gage section length and diameter of 35 and 6·35 mm, respectively.

computer. Test temperatures were 1316, 1371, and 1399°C, and examined static tensile stresses ranged between 25 and 190 MPa. All these specimens conclusively were in a secondary creep regime at failure or they were interrupted after a minimum of 150 h of secondary creep (the latter only pertinent for creep tests involving a low-valued stress). The tensile creep histories showed a primary and secondary creep region. Tertiary creep behavior was never observed. The minimum tensile creep rate from the secondary creep region was determined as a function of stress and temperature for each specimen.

Transmission electron microscopy (TEM) studies were performed on five pairs of creep tested specimens. The specimens from each pair were creep tested at the same temperature and magnitude of stress; however, one specimen was tested in tension and the other in compression. The five pairs of conditions were 1316°C:|125| MPa, 1371°C:|30 MPa, 1371°C:|200 MPa* 1399°C: |25| MPa, and 1399°C:|100| MPa. TEM foils were prepared from the bulk of the crept specimens and from planes parallel to the loading axis. Foils were also prepared from as-received material and served as the reference.

3 Results and Discussion

3.1 Asymmetric creep response

Minimum creep rates were always faster in tension than in compression for an equal magnitude of stress. Examples of this creep asymmetry are illustrated in Figs 3–7 for 1316C:≤125| MPa, 1371°C|:|30 MPa, 1371°C:|200| MPa, 1399C:|25| k MPa, and 1399°C:|100| MPa, respectively. The creep histories in Figs 3–7 show the tensile and compressive curves start to diverge right from the beginning of the test. Primary and secondary creep regimes were observed for both tension and compression creep tests with primary creep typically ending around 50–75 h for all temperatures and stresses. The conversion of α-Si_3N_4 to β-Si_3N_4 at these test temperatures likely contributed to the accumulation of some of the primary creep strain in NT154.[24] The ratio of the minimum creep rate in tension to that in compression for the same magnitude of stress increased with increase in magnitude of stress. For example, the creep rate in tension was approximately 20 times faster than that in compression at 1371°C:|200| MPa (Fig. 5), while only approximately twice as fast at 1371°C: |30| MPa (Fig. 4). This trend was independent of temperature (1399°C in Figs 6 and 7). Although magnitudes of stress less than 25 MPa were not examined due to experimental limitations, there was no indication from the presently generated data to suggest that the magnitudes of tensile and compressive creep rates should be equal for equal

*A tensile creep test was not conducted at 200 MPa, but at 190 MPa. Consequently, the tensile creep test results at 190 MPa are compared to the compressive creep test results at 200 MPa.

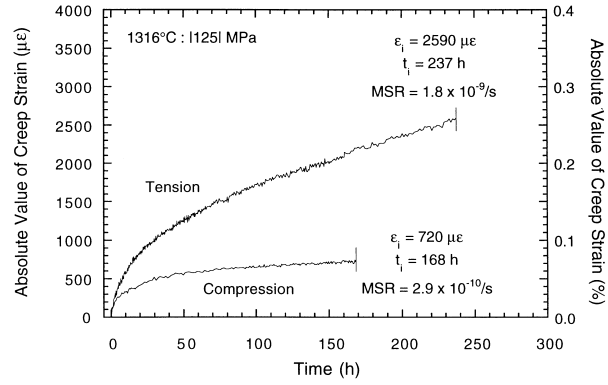

Fig. 3. Comparison of tensile and compressive creep histories for specimens tested at 1316°C and 125 MPa. Symbols: ε = strain, t = time, MSR = minimum strain rate, i = interrupt, f = failure.

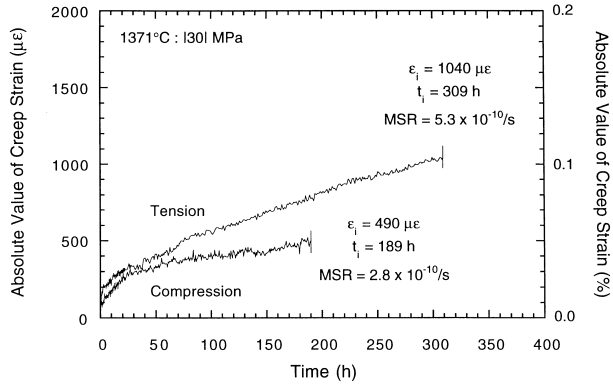

Fig. 4. Comparison of tensile and compressive creep histories for specimens tested at 1371°C and 30 MPa. ε = strain, t = time, MSR = minimum strain rate, i = interrupt, f = failure.

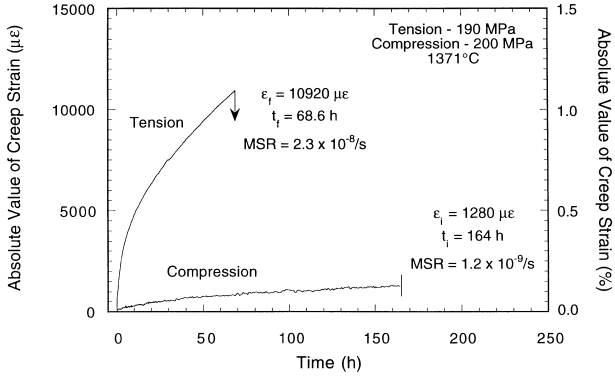

Fig. 5. Comparison of tensile and compressive creep histories for specimens tested at 1371°C and 190 MPa (tension) and 200 MPa (compression). Symbols: ε = strain, t = time, MSR = minimum strain rate, i = interrupt, f = failure.

magnitudes of applied stress other than at zero applied stress and zero creep rate. The minimum creep rates as a function of stress and temperature are listed in Table 1.

A single function was sought to represent the minimum creep rate as a function of stress and temperature and which did not require conditional or *a priori* knowledge of the sign of stress. Such a model would need to be amenable for use with commercial finite element analysis software. The sought function would also address the linear dependence of compressive creep rate on compressive stress and represent the tensile creep rate being exponentially dependent on tensile stress. The resulting empirical function was an additive combination of eqns (1) and (3) and had the form:

$$d\varepsilon/dt = [A\sigma + B\sigma \exp(C\sigma)] \exp(-Q/RT) \qquad (4)$$

where: $d\varepsilon/dt$ is the minimum creep rate (− for compression, + for tension); A, B, and C are constants; σ is stress (− for compression, + for tension); Q is the activation energy constant; R is the gas constant; and T is absolute temperature. For compressive or negative stress, the first term in the bracketed expression in eqn (4) dominates* while the second term in the brackets dominates for tensile or positive stress. The form of eqn (4) also mathematically addresses the boundary condition that there must be zero creep rate for zero stress. A single activation energy term in eqn (4) assumes it

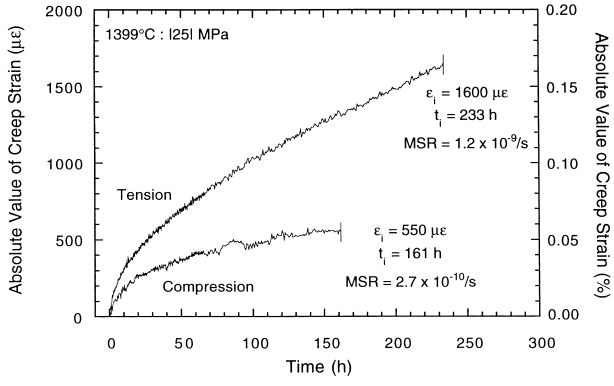

Fig. 6. Comparison of tensile and compressive creep histories for specimens tested at 1399°C and 25 MPa. Symbols: ε = strain, t = time, MSR = minimum strain rate, i = interrupt, f = failure.

*This is true for conditions when B is approximately equal to or less than $3A$ (or $B/3A < 1$). As $B/3A$ becomes greater than one, the validity of the assumption that eqn (4) approximates linear dependence of compressive creep rate on compressive stress decreases because the exponential stress term in eqn (4) starts to dominate. As an illustration of this, the slight 'waviness' in the fits to the compressive creep data in Figs 8(b), 9(b), and 10(b) exists because B is approximately 2–2·5 times as large as A. As $B/3A \ll 1$ the fit of eqn (4) to compressive creep data using get more linear.

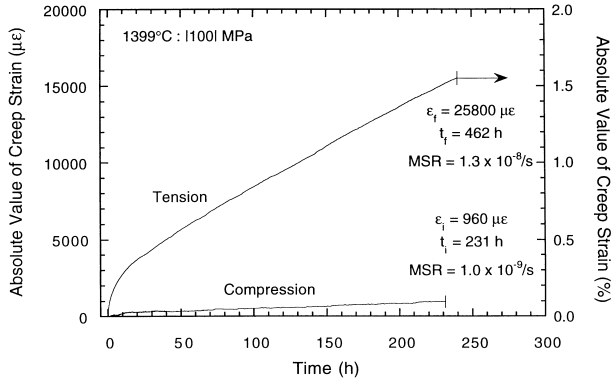

Fig. 7. Comparison of tensile and compressive creep histories for specimens tested at 1399°C and 100 MPa. Symbols ε = strain, t = time, MSR = minimum strain rate, i = interrupt, f = failure.

is equal-valued for both compressive and tensile creep deformation. Lastly, because the square-bracketed terms in eqn (4) are summed, multiple linear regression cannot be performed so nonlinear regression analysis was required.

The creep data in Table 1 were first fitted to eqn (4) using nonlinear regression with the assumption that variance was constant. This assumption is typically made in the literature in which creep data are regressed against one of the models represented in eqns (1)–(3). The nonlinear regression analysis was performed using the 'Splus' function described in Ref. 25. To promote convergence of the analysis, plausible values for the constants A, B, C, and Q were required for initial input. Linear regression of the compressive creep data of $\log[(d\varepsilon/dt)/\sigma]$ on $-1/RT$ was used to obtain initial values for A and Q. Initial estimates of B, C, and Q were obtained using multiple linear regression of $\log[(d\varepsilon/dt)/\sigma]$ on σ and $-1/RT$ with the tensile creep data. The Q values from the two analyses were then averaged. The resulting initial values used for the nonlinear regression were $A = 3{\cdot}93133 \times 10^{12}\,\mathrm{MPa^{-1}\,s^{-1}}$, $B = 3{\cdot}20211 \times 10^{14}\,\mathrm{MPa^{1}\,s^{-1}}$, $C = 0{\cdot}0117\,\mathrm{MPa^{-1}}$, and $Q = 490{\cdot}3\,\mathrm{kJ\ mol.^{-1}}$

The resulting nonlinear regression fit (constant-variance-assumption or 'unweighted analysis') to the data is shown in Fig. 8(a) and (b). The estimates of the constants which resulted from the unweighted nonlinear regression analysis of eqn (4) to the data in Table 1 were $A = 1{\cdot}086 \times 10^{12}\,\mathrm{MPa^{-1}\,s^{-1}}$, $B = 1{\cdot}838 \times 10^{12}\,\mathrm{MPa^{-1}\,s^{-1}}$ $C = 0{\cdot}01879\,\mathrm{MPa^{-1}}$, and $Q = 740\,\mathrm{kJ\ mol^{-1}}$. The activation energy value of 740 kJ mol for the unweighted nonlinear regression fit is consistent with activation energies measured for viscosity of oxynitride glasses[26] as well as the sublimation of Si_3N_4.[27] These four values and their 95% confidence intervals are listed in Table 2. In order to plot all the data and the fitted function on a single graph, the temperature compensated creep rate (TCCR) was plotted

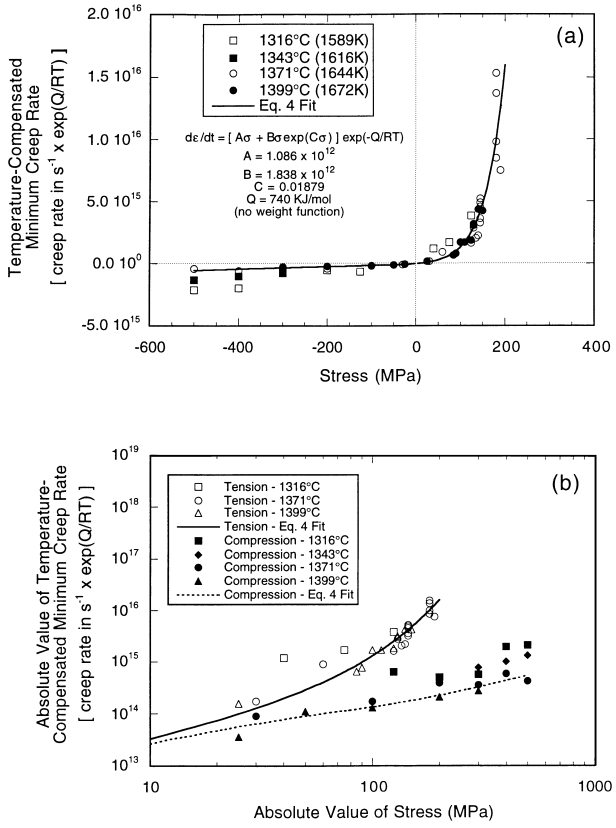

Fig. 8. Fitted function using eqn (4) of temperature compensated minimum creep rate as a function of stress (a) linear-linear representation, and (b) log–log representation of absolute values. This function assumed that the variance was constant (or no weight function was applied).

as a function of stress in Fig. 8(a) and (b). The TCCR was determined by dividing both sides of eqn (4) by the exponential temperature term {exp(-Q/RT)}, with the result being TCCR = $d\varepsilon/dt^{\bullet}$ exp(Q/RT). A linear-linear plot of TCCR and stress is shown in Fig. 8(a) which illustrates the model's exponential dependence of TCCR on tensile stress and its linear dependence of TCCR on compressive stress. A log–log plot of creep rate and stress is a more recognizable graphical representation, so the absolute TCCR were plotted as a function of absolute stress in Fig. 8(b). Like Fig. 8(a), the linear and exponential dependence of TCCR on compressive and tensile stress, respectively, are evident. The fitted compressive creep rate dependence on compressive stress is not strictly linear because of the slight influence of the exponential stress term in eqn (4).

The analysis of the residuals from the unweighted nonlinear regression fit shown in Fig. 8(a) and (b) revealed that the variance was not constant. Greater variability was observed for larger values of creep rate. Consequently, a statistical 'weight function' was introduced which adjusted for this non-constant variance. The pattern in the residuals indicated that the variability in creep rate was proportional to the square of the expected creep rate as defined by the regression function in eqn (4) {i.e., variance(creep rate) = [ϕ (expected creep rate)]^2, where ϕ is an unknown constant estimated from the residuals}. When the variance is not constant, an iterative weighed least squares (IWLS) algorithm can be used for nonlinear regression.[28] If the dependent variable is in the exponential family, then this leads to maximum likelihood estimates of the unknown parameters. The IWLS can also be used under the second moment assumptions described here to obtain maximum quasi-likelihood estimates.[29] The weighted regression estimates based on eqn (4). were computed using IWLS. The same initial values for the constants A, B, C, and Q used for the unweighted nonlinear regression analysis were also used for the weighted analysis.

The resulting weighted nonlinear regression fit (non-constant variance adjusted for) to the data in Table 1 is shown in Fig. 9(a) and (b). The constants in eqn (4) resulting from the weighted nonlinear regression were $A = 165{\cdot}2\,\mathrm{MPa^{-1}s^{-1}}$, $B = 394{\cdot}7$ $\mathrm{MPa^{-1}s^{-1}}$, $C = 0{\cdot}01488\,\mathrm{MPa^{-1}}$, and $Q = 427\,\mathrm{kJ\,mol^{-1}}$. These four parameters and their 95% confidence are listed in Table 2. The 95% confidence intervals for these four constants are narrower than the intervals for the determined constants from the unweighted function which is illustrative of the improved fit to the creep data. The Q value from the weighted-analysis is consistent with matter transport through the intergranular amorphous phase by the solution-reprecipitation mechanism.[31] This weighted-analysis activation energy value was different than the unweighted-analysis activation energy (740 kJ mol^{-1}); however, more confidence is

Table 2. Results of nonlinear regression using unweighted and weighted functions

Parameter	*Unweighted function value*	*± 95% confidence interval*	*Weighted function value*	*± 95% confidence interval*
A (MPa^{-1} s^{-1})	$1{\cdot}086\times10^{1/2}$	$4{\cdot}878\times10^{5}$ $2{\cdot}418\times10^{18}$	$1{\cdot}652\times10^{2}$	$3{\cdot}883\times10^{-1}$ $7{\cdot}027\times10^{4}$
B (MPa^{-1} s^{-1})	$1{\cdot}838\times10^{1/2}$	$1{\cdot}678\times10^{6}$ $2{\cdot}012\times10^{18}$	$3{\cdot}947\times10^{2}$	$1{\cdot}069\times10^{o}$ $1{\cdot}457\times10^{5}$
C (MPa^{-1})	0·01879	0·01362 0·02396	0·01488	0·01246 0·01730
Q (kJ mol^{-1})	740	541 939	427	345 509

placed in the weighted-analysis value of 427 kJ mol^{-1} due to its improved statistical correlation. In almost all literature involving creep deformation, creep rate date are regressed against a function of stress assuming a constant variance: the identifications in the present study that variance was *non-constant* and that unweighted and weighted results produce different values of activation energy (and subsequent description of operating mechanisms) indicates that caution should be exercised with interpreting reported unweighted creep rate/stress analysis. Graphical analysis of the Pearson residuals[30] from the nonlinear regression indicated that this variance assumption for the weighted analysis was appropriate for the creep rate data, and provided a clear improvement over the constant variance assumption. A linear-linear plot of TCCR and stress is shown in Fig. 9(a) and a log–log plot of the absolute TCCR are plotted as a function of absolute stress in Fig. 9(b). The visual differences in the results between the unweighted and weighted nonlinear regression analysis are most obvious in the log–log plots of Figs 8(b) and 9(b). The fitted functions for each show the weighted function in Fig. 9(b) to fit the data better.

The log–log weighted functions for the absolute tensile and compressive creep rates as a function of absolute stress and temperature are illustrated in Fig. 10(a) and (b), respectively. Figure 10(a) shows the weighted function appears to fit the 1371 and 1399°C tensile creep data better than the 1316°C data. Likewise, the weighted function fits the compressive creep data better for the same two temperatures. The seemingly lack of correlation between the fit and the 1316°C creep data was likely due to the relatively low number of data points at this temperature, which provided less influence on the determination of the four constants from of the weighted nonlinear regression analysis.

3.2 Differences in cavitation stress dependence

Post-testing microstructural analysis using TEM revealed that differences in the amounts of tensile- and compressive-stress-induced cavitation accounted for the creep strain asymmetry between them. A summary of the TEM results are listed in Table 3. Multigrain junction cavities formed in all tensile crept specimens, and concentrations were greatest in tensile specimens tested at 1371°C:190 MPa (Fig. 11) and 1399°C:100 MPa. Much lower concentrations of multigrain junction cavities were present in the specimen tensile tested at 1316°C: 125 MPa. A small concentration of multigrain

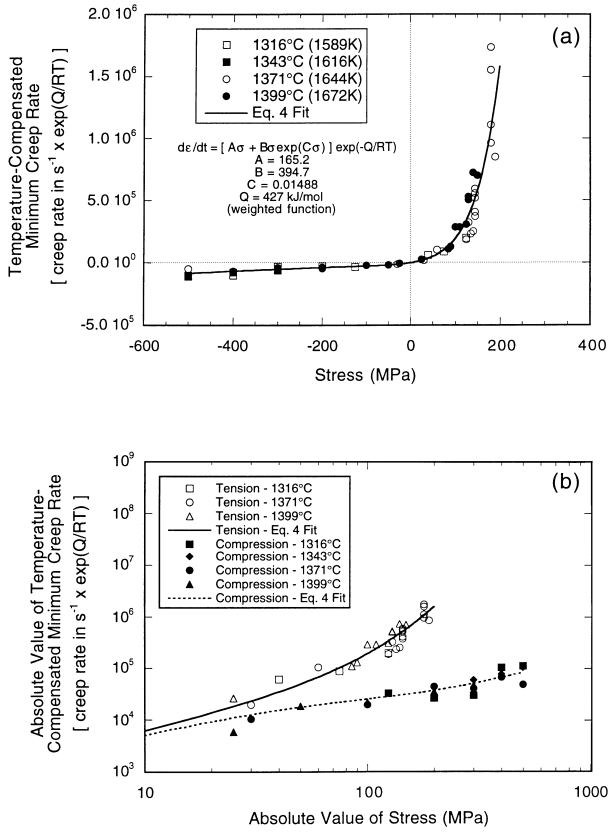

Fig. 9. Fitted (with weight function) function using eqn (4) of temperature compensated minimum creep rate as a function of stress (a) linear-linear representation, and (b) log–log representation of absolute values. This function acknowledged that the variance was not constant (weight function applied).

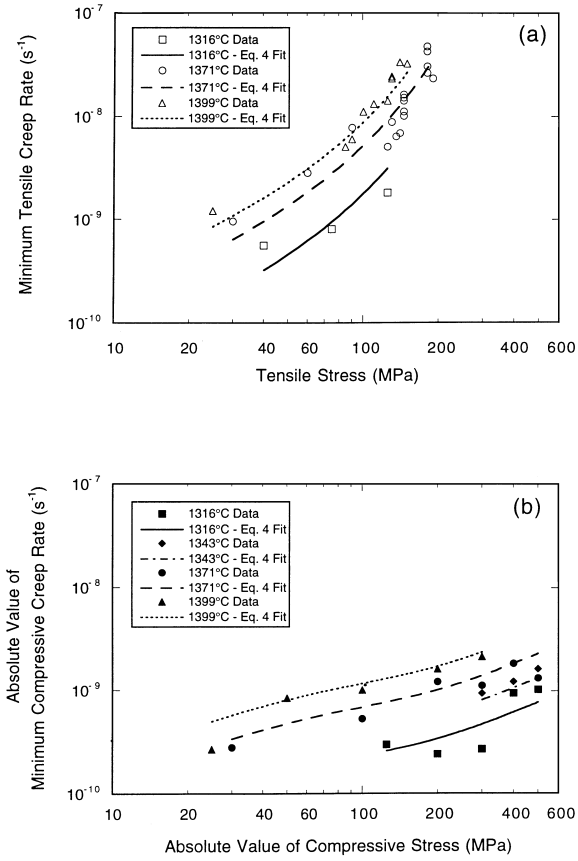

Fig. 10. Creep rate as a function of temperature and (a) tensile stress and (b) compressive stress. The shown fitted functions use the weighted parameters shown in Table 2 and Fig. 9(a) and (b).

Table 3. Summary description of TEM results

Temperature (°C)	*Stress (MPa)*	*TEM observations*
1316	125	Some multigrain junction cavities observed
	−125	No observable difference from as-received microstructure
1371	30	Had some relatively small multigrain junction cavities, but needed to look for
	−30	No observable difference from as-received microstructure
1371	190	High concentration of multigrain junction cavities and some two-grain lenticular-shaped cavities
	−200	Some multigrain junction cavities observed
1399	25	Had some multigrain junction cavities, but needed to look for
	−25	No observable difference from as-received microstructure
1399	100	High concentration of multigrain junction cavities and some two-grain lenticular-shaped cavities
	−100	Some multigrain junction cavities observed

junction cavities were present in the specimens tensile tested at 1371°C:30 MPa and 1399°C: 25 MPa; however, much more extra imaging time was necessary in order to locate them (unlike for the other three examined tensile crept specimens). Multigrain junction cavities also formed in compressively crept specimens tested at 1371°C: 200 MPa and 1399°C:-100 MPa (see Fig. 12) but their concentrations were far less than their tensile specimen counterparts and were also less than the cavity concentration in the tensile crept specimen at 1316°C:125 MPa.

In addition to cavity-concentration differences, trends in cavity-type, size, and location also provided insights into the tensile and compressive creep deformation behavior. Multigrain junction cavities always formed in regions containing numerous equiaxed silicon nitride grains. The size of multigrain junction cavities appeared to be independent of test condition (and accumulated creep strain), with only the resulting cavity concentrations being conclusively different among them. Two-grain lenticular-shaped cavities were only found in the tensile specimens tested at 1371°C:190 MPa and 1399°C:100 MPa (see Fig. 13). The size of the two-grain lenticular-shaped cavities were smaller than the multigrain junction cavities, and were always found between two relatively large silicon nitride grains (grains which were usually acicular-shaped). Additionally, the length of the major axis of the lenticular cavities were always much less than the facet sizes of the two adjacent grains each grew into. If cavity formation were indeed initiated in the specimens tested at 1316°C: −125 MPa, 1371°C:30 MPa, 1371°C:−30 MPa, 1399°C:25 MPa, and 1399°C:−25 MPa, then their concentrations were so low that they were indistinguishable from the relatively low concentration

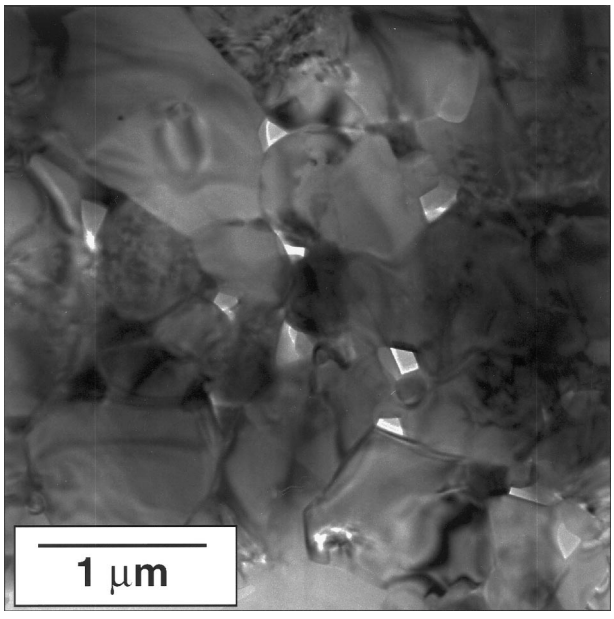

Fig. 11. All tensile creep specimens contained multigrain junction cavities, while those tested at high stresses contained much larger concentrations of them. The shown microstructure was from the specimen tested in tension at 190 MPa and 1371°C (creep history shown in Fig. 5).

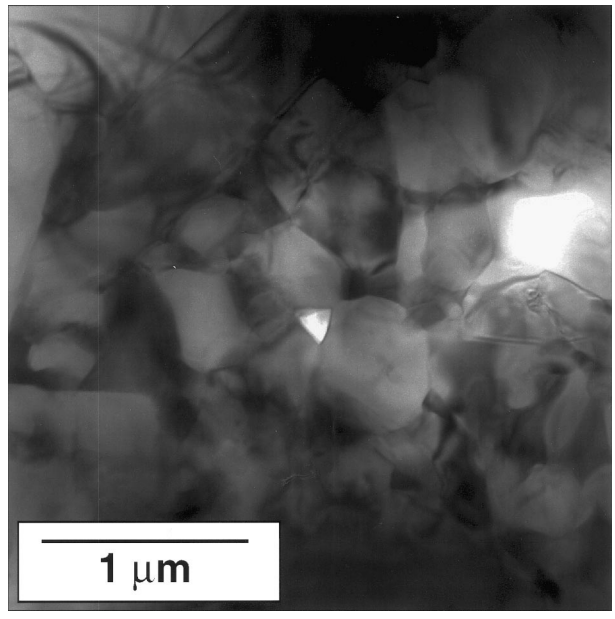

Fig. 12. Compression creep specimens tested at high stresses had a relatively low concentration of multigrain junction cavities. The shown microstructure was from the specimen tested in compression at 200 MPa and 1371°C (creep history shown in Fig. 5).

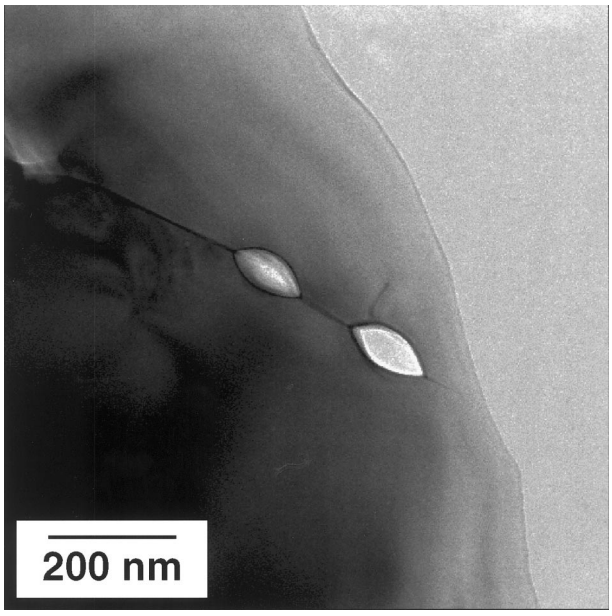

Fig. 13. Only specimens crept in tension at relatively high stresses contained two-grain, lenticular-shaped cavities. The shown microstructure was from the specimen tested in tension at 100 MPa and 1399°C (creep history shown in Fig. 7).

of remnant porosity observed in the as-received material. These findings are consistent with the observation that cavitation accounts for the majority of creep strain accumulation in silicon nitride.[2]

The relative amounts of accumulated creep strain illustrated in Figs 3–7 were consistent with the amount of cavitation observed with TEM. Specimens tested at conditions of 1316°C: −125 MPa, 1371°C:−30 MPa, and 1399°C:−25 MPa accumulated less than 0·1% creep strain and their microstructures showed no distinguishable cavity formation. A threshold strain has been described in the literature which is a critical strain which (1) first needs be exceeded by total creep strain prior to the initiation of cavitation[4,32,33] or (2) needs to be exhausted by the viscous flow of the secondary phase {which occurs early on in creep deformation}.[34] The small amounts of strain accumulated by these three specimens suggests that such a threshold was not exceeded because multigrain junction cavities did not form. The specimens which accumulated more than 0·1% creep strain (either for tension or compression) contained multigrain junction cavities. Two-grain lenticular shaped cavities were observed in the tensile specimens tested at 1371°C/190 MPa and 1399°C/100 MPa (both accumulated in excess of 1% creep strain). Such lenticular cavities were not observed in the tensile specimen tested at 1316°C:125 MPa which indicates their formation was due to the combination of relatively high temperature and stress.

An explanation of the asymmetry in creep accumulation between tension and compression for equal magnitudes of stress and temperature has been previously examined, but the results in the present study contribute additional insight to the overall understanding. Luecke *et al.*,[2] attributed the asymmetry in NT154 Si_3N_4 to the dominance of cavity formation in tension (with secondary phase flow away from them) and the dominance of the more sluggish solution-reprecipitation mechanism in compression. Although solution-reprecipitation may have been operative during compression creep, the results in the present study show that cavity formation can also occur during compression creep, so solution-reprecipitation cannot be exclusive to compressive creep deformation at all stresses and temperatures.

4 Conclusions

The tensile and compressive creep of an yttria-containing hot-isostatically-pressed silicon nitride were examined at several temperatures between 1316 and 1399°C and found to have different stress dependencies. Creep rates were always faster in tension than compression for an equal magnitude of stress even for a stress as low as 25 MPa. The magnitude of accumulated tensile and creep strain diverged at test initiation for equal magnitudes of stress. An empirical model was formulated which represented the creep rate as a function of temperature for both tensile and compressive stress, and which depicted the asymmetric creep deformation using exponential and linear dependence on tensile and compressive stress, respectively. The formulated model represented creep deformation rate for both tensile and compressive stresses without conditional or *a priori* knowledge of the sign of stress, which is unlike other models used with polycrystalline ceramics which represent *either* tensile or compressive creep deformation, but not both. A weight function was introduced which statistically improved the quality of the model's fit to the experimental data.

Multigrain junction cavities formed in all tensile crept specimens, with larger concentrations found in tensile specimens which accumulated greater amounts of tensile creep strain. Multigrain cavities also formed in compressively crept specimens tested at relatively high temperatures and stresses, but their concentrations were far less than their tensile specimen counterparts tested at the same magnitude of stress. Multigrain junction cavities tended to form in regions containing numerous equiaxed silicon nitride grains. The sizes of multigrain junction cavities appeared to be independent of test condition (and accumulated creep strain); only the resulting cavity concentrations between test conditions were

conclusively different. Two-grain lenticular-shaped cavities were only found in the tensile specimens which were tested under a combination of relatively high tensile stress and temperature.

Acknowledgements

The authors are indebted to D. R. Johnson (Program Manager, Ceramic Technology Project) and C. R. Brinkman (Technical Monitor, W.B.S. Element 3.2.2.3) for their support of this work. The authors wish to thank C.-H. Hsueh and R. W. Swindeman for their reviews of this article and for their helpful suggestions.

References

1. Ferber, M. K., Jenkins, M. G. and Tennery, V. J., Comparison of tension, compression, and flexure creep for alumina and silicon nitride ceramics. *Ceram. Eng. Sci. Proc*, 1990, **11**(7–8), 1028–1045.
2. Luecke, W. E., Wiederhorn, S. M., Hockey, B. J., Krause, Jr, R. F. and Long, G. G., Cavitation contributes substantially to tensile creep in silicon nitride. *J. Am. Ceram. Soc*, 1995, **78**(8), 2085–2096.
3. Norton, F. H., *The Creep of Steel at High Temperature* McGraw Hill, New York, 1929.
4. Luecke, W. E., Wiederhorn, S. M., Hockey, B. J. and Long, G. G., Cavity evolution during tensile creep of Si_3N_4. *Mater. Res. Soc. Symp. Proc*, 19983, **287**, 467–472.
5. Crampon, J., Duclos, R. and Rakotoharisoa, N., Compression creep of $Si_3N_4/MgAl_2O_4$ alloys. *J. Mat. Sci.*, 1990, **25**, 1203–1208.
6. Coble, R. L., A model for boundary diffusion controlled creep in polycrystalline materials. *J. Appl. Phys*, 1963, **34**, 1679–1682.
7. Menon, M. N., Fang, H. T., Wu, D. C., Jenkins, M. G., Ferber, M. K., More, K. L., Hubbard, C. R. and Nolan, T. A., Creep and stress rupture behavior of an advanced silicon nitride: part I, experimental observations. *J. Am. Ceram. Soc.*, 1994, **77**(5), 1217–1227.
8. Menon, M. N., Fang, H. T., Wu, D. C., Jenkins, M. G. and Ferber, M. K., Creep and stress rupture behavior of an advanced silicon nitride: part II, creep rate behavior. *J. Am. Ceram. Soc.*, 1994, **77**(5), 1228–1234.
9. Gasdaska, C. J., Tensile creep in an *in situ* reinforced silicon nitride. *J. Am. Cer. Soc*, 1994, **77**, 2408–2418.
10. Wiederhorn, S. M., Hockey, B. J., Cranmer, D. C. and Yeckley, R., Transient creep behavior of hot isostatically pressed silicon nitride. *J. Mat. Sci*, 1993, **28**, 445–453.
11. Ferber, M. K., Jenkins, M. G., Nolan, T. A. and Yeckley, R. L., Comparison of the creep and creep rupture performance of two HIPed silicon nitride ceramics. *J. Am. Cer. Soc*, 1994, **77**, 657–665.
12. Ferber, M. K. and Wereszczak, A. A., Modeling of the time-dependent failure of structural ceramics at elevated temperatures, to be submitted to *J. Am. Cer. Soc.*.
13. Jonas, J. J., The back stress in high temperature deformation. *Acta Met*, 1969, **17**, 397–405.
14. Sellars, C. M. and Tegart, W. J. Mc G., La relation entre la rérsistance et la structure dans la déformation à chaud. *Mém. Sci. Rev. Met*, 1996, **63**, 731–746.
15. Hazime, R. M. and White, C. S., Multiaxial internal variable modeling of the creep deformation and fraction of an advanced silicon nitride. *Cer. Engrg. Sci. Proc*, 1997, **18**, 455–465.
16. Wiederhorn, S. M. and Luecke, W. E., Creep of silicon nitride. In *Computer-Aided Design of High-Temperature Materials* ed. A. Pechenik, R. K. Kalia and P. Vashishta, Oxford University Press, 1998.
17. Krause, Jr, R. F., Luecke, W. E., French, J. D., Hockey, B. J. and Wiederhorn, S. M., Tensile creep and rupture of silicon nitride submitted to *J. Am. Cer. Soc.*
18. Luecke, W. E. and Wiederhorn, S. M., A new model for tensile creep of silicon nitride, to be submitted to the *J. Am. Cer. Soc.*
19. Chuang, T.-J., Estimation of power-law creep parameters from bend test data. *J. Mat. Sci*, 1986, **21**, 165–175.
20. Lim, H. J., Jung, J. W., Han, D. B. and Kim, K. T., A finite element model for asymmetric creep behavior of ceramics. *Mat. Sci. Engrg*, 1977, **A224**, 125–130.
21. *Standard Test Method for Flexural Strength of Advanced Ceramics at Ambient Temperature*, ASTM C1161, Vol. 15·01, Annual Book of ASTM Standards, American Society for Testing and Materials, West Conshohocken, PA, 1997.
22. Life Prediction Methodology for Ceramic Components of Advanced Heat Engines, Phase 1, Prepared by Allied Signal Engines, Phoenix, AZ, ORNL/Sub/89-SC674/1, DOE Office of Transportation Technologies, March 1995.
23. Birch, J. M., Wilshire, B., Owen, D. J. R. and Shantaram, D., The influence of stress distribution on the deformation and fracture behaviour of ceramic materials under compression creep conditions. *J. Mat. Sci*, 1976, **11**, 1817–1825.
24. Wereszczak, A. A., Kirkland, T. P., Ferber, M. K., Watkins, T. R. and Yeckley, R. L., The effects of residual phase on the creep performance at 1370°C of yttria-doped HIPed silicon nitride. *J. Mat. Sci.*, 1998, **33**, 2053–2060.
25. Bates, D. M. and Chambers, J. M., Nonlinear models. In *Statistical Models in S*, ed. J. M Chambers and T. J. Hastie. Wadsworth and Brooks/Cole, Pacific Grove, CA, 1992, Chapter 10.
26. Rouxel, T., Besson, J.-L., Gault, C., Goursat, P., Leigh, M. and Hampshire, D., Viscosity and young's modulus of an oxynitride glass. *J. Mater. Sci. Lett*, 1989, **8**(10), 1158–1160.
27. Pehlke, R. D. and Elliot, J. F., High temperature thermodynamics of the silicon, nitrogen, silicon nitride system. *Trans. Metall. Soc. AIME*, 1959, **215**, 781–792.
28. Charnes, A., Frome, E. L. and Yu, P. L., The equivalence of generalized least squares and maximum likelihood estimates in the exponential family. *J. Am. Stat. Assoc.*, 1976, **71**, 169–171.
29. McCullagh, P., Quasi-likelihood Functions. *The Annals of Statistics*, 1983, **11**, 59–67.
30. McCullagh, P. and Nelder, J. A., *Generalized Linear Models*. Chapman and Hall, London, 1989.
31. Raj, R. and Morgan, P. E. D., Activation energies for densification, creep, and grain-boundary sliding in nitrogen ceramics. *J. Am. Cer. Soc.*, 1981, **64**, C143.
32. Lin, C.-K. J., Jenkins, M. G. and Ferber, M. K., Cyclic fatigue of hot isostatically pressed silicon nitride at elevated temperatures. *J. Mat. Sci.*, 1994, **29**, 3517–3526.
33. Wereszczak, A. A., Ferber, M. K., Kirkland, T. P. and Lin, C.-K. J., Effect of cyclic loading on the creep performance of silicon nitride. *J. Engrg. Gas Turb. Power*, 1996, **118**, 251–256.
34. Jin, Q., Ning, X.-G., Wilkinson, D. S. and Weatherly, G. C., Redistribution of a grain-boundary glass phase during creep of silicon nitride ceramics. *J. Am. Cer. Soc.*, 1997, **80**, 685–691.